ACS APPLIED MATERIALS & INTERFACES

Research Article

www.acsami.org

Efficient 3D Conducting Networks Built by Graphene Sheets and Carbon Nanoparticles for High-Performance Silicon Anode

Xiaosi Zhou, Ya-Xia Yin, An-Min Cao, Li-Jun Wan, and Yu-Guo Guo*

Beijing National Laboratory for Molecular Sciences (BNLMS), Institute of Chemistry, Chinese Academy of Sciences (CAS), Beijing 100190, P.R. China

Supporting Information

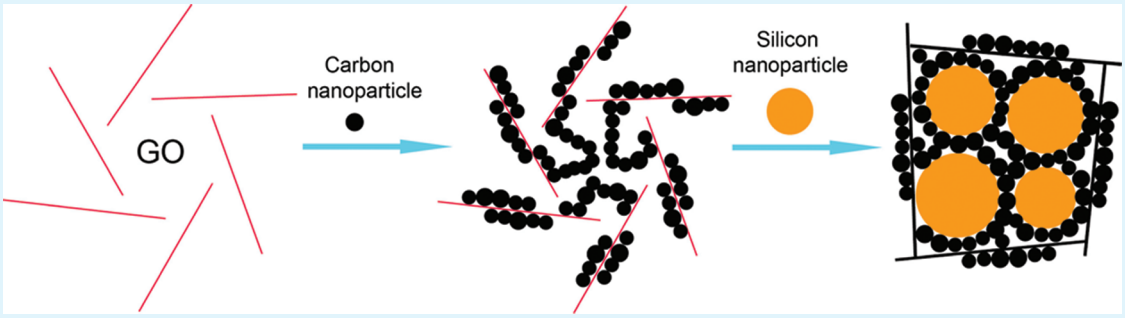

ABSTRACT: The utilization of silicon particles as anode materials for lithium-ion batteries is hindered by their low intrinsic electric conductivity and large volume changes during cycling. Here we report a novel Si nanoparticle−carbon nanoparticle/graphene composite, in which the addition of carbon nanoparticles can effectively alleviate the aggregation of Si nanoparticles by separating them from each other, and help graphene sheets build efficient 3D conducting networks for Si nanoparticles. Such Si−C/G composite shows much improved electrochemical properties in terms of specific capacity and cycling performance (ca. 1521 mA h g^{-1} at 0.2 C after 200 cycles), as well as a favorable high-rate capability.

KEYWORDS: *lithium-ion batteries, 3D conducting networks, silicon, graphene, carbon nanoparticles, anode materials*

INTRODUCTION

Tremendous attention has been paid to electrochemical devices for energy conversion and storage with advantages such as safety, low cost, and high energy density, as well as long cycle life. These devices have potential uses in powering future portable electronics and electric vehicles (EVs), and also in large-scale energy storage. In terms of high energy density, lithium-ion batteries are the most promising candidate among these devices.[1−9] Because the performance of lithium-ion batteries is primarily determined by electrode materials, pursuing high-capacity anode or cathode materials is of great interest. Silicon-based anodes, because of its numerous appealing characteristics such as high gravimetric capacity (~4200 mA h g^{-1}), low working potential (~0.5 V vs Li^+/Li), abundance and environmental benignity, has attracted considerable interest as a promising candidate for replacing the commercial graphite anode,[10−15] which exhibits relatively low theoretical capacity of 372 mA h g^{-1}.

However, before the full utilization of Si as a practical anode material, there are still two major problems needed be addressed, i.e., the low intrinsic electronic conductivity of Si and its dramatic volume changes (>300%) during cycling. It is well-known that the Li alloying/dealloying processes will produce significant mechanical stress within the materials, resulting in cracking and pulverization of Si, electrical disconnection from the current collector, and eventual capacity fading.[16] Enormous efforts have been made to overcome these problems by using nanostructured Si including nanowires,[17] nanotubes,[18] nanocables,[19] and nanospheres,[20] and coating electronically conductive agents, such as carbon,[10,13,21,22] graphene,[23−25] Ag,[16] conducting polymer.[26] In these strategies, huge volume changes can be effectively cushioned because the introduced free volume and robust coatings can, as it did, retain the electrode integrity. However, it remains challenging to achieve long cycle life and high capacity of Si anode materials in large scale via facile approaches.

Graphene has been used to coat electroactive materials by researchers due to its high electronic conductivity, superior mechanical strength and flexibility.[27−30] According to its intrinsic electronic structure, the adjacent portions of graphene sheets generated from the reduction of graphene oxide are easily reconstituted to form a network of graphite, which performs as a strong framework to encapsulate the nanoparticles such as Si and oxides.[23,31,32] Therefore, the utilization of graphene is promising to accommodate the volume variations of nanoparticles and even prevent the breakage of electrode integrity. Recently, we have developed a novel technique to fabricate Si nanoparticles intercalated in graphene

Received: March 30, 2012
Accepted: May 6, 2012
Published: May 6, 2012

   dx.doi.org/10.1021/am3005576 | ACS Appl. Mater. Interfaces 2012, 4, 2824−2828

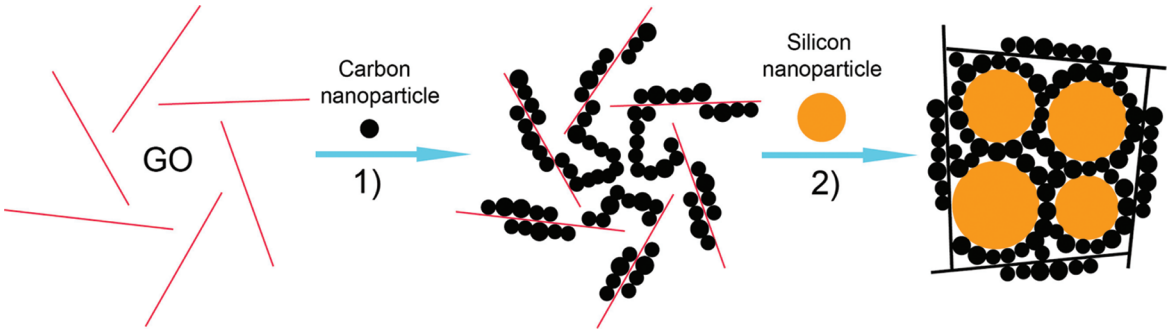

Figure 1. Schematic illustration of preparation of the Si−C/G composite, black line (graphene sheets).

sheets by combining two processes of freeze-drying and thermal reduction together.[24] From a low concentration of Si nanoparticles aqueous suspension, we obtained a composite of Si nanoparticles inserted in graphene sheets with less aggregation. However, as the concentration of Si nanoparticles increases, the conglomeration of Si nanoparticles becomes inevitable due to the low hydrophilicity of Si nanoparticles. The electronic conductivity of such aggregated Si nanoparticles will decrease because of the less contact between graphene and Si nanoparticles, leading to a bad battery performance.

Here, we propose and realize an optimized design of novel Si nanoparticles-carbon nanoparticles/graphene composite (hereafter abbreviated as Si−C/G composite) to solve the aggregation problem. Carbon nanoparticles are selected as an effective component to promote the electronic conductivity of the composite. Compared to the Si/G composite, the existence of additional carbon nanoparticles can contribute in the following two aspects. First, it can effectively alleviate the aggregation of Si nanoparticles by separating them from each other. Second, the contact between carbon nanoparticles and Si nanoparticles will afford more channels for electronic conducting. The combination of graphene sheets and carbon nanoparticles together can build an efficient 3D conducting network to obtain a high-performance Si-based anode through an easy and efficient use of Si nanoparticles. In addition, the graphene sheet prepared in this method can act as an effective framework to buffer the large volume changes during battery cycling.[26] Electrochemical measurements on lithium-ion batteries revealed that the Si−C/G composite not only delivers an improved reversible capacity of 1521 mA h g^{-1} at 0.2 C after 200 cycles but also shows a good high-rate capability.

EXPERIMENTAL SECTION

Fabrication of Graphite Oxide. The graphite oxide was produced by a modified Hummers' method as reported elsewhere.[33]

Synthesis of Silicon Nanoparticle−Carbon Nanoparticle/Graphene Composite. Four milliliters of graphite oxide aqueous suspension (10.0 mg mL^{-1}) was diluted to 1.0 mg mL^{-1} with double distilled water, then 40 mg of carbon nanoparticles (~40 nm in diameter, Super-P, Timcal) was added into the graphite oxide aqueous suspension and the obtained mixture was sonicated for 20 min to achieve a black homogeneous carbon nanoparticles/graphene oxide aqueous suspension. Afterward, 160 mg of silicon nanoparticles (<300 nm, Top Vendor Science & Technology Co., Ltd.) were dispersed in 20 mL of water via 40 min sonication (KQ3200DE, 40 kHz). Then, the achieved Si nanoparticles aqueous suspension was added into the above carbon nanoparticles/graphene oxide aqueous suspension, and the obtained mixture was sonicated for 10 min to obtain a uniform Si nanoparticles-carbon nanoparticles/graphene oxide aqueous suspension. The resulting homogeneous aqueous suspension was lyophilized, followed by reduction in a crucible in a tube furnace at 700 °C for 2 h under H_2 (5 vol%)/Ar (95 vol%) atmosphere with a heating rate of 2 °C min^{-1}, treatment with 20% HF water/ethanol solution, and drying under vacuum at 80 °C to finally obtain Si−C/G composite.

Synthesis of Silicon Nanoparticle/Graphene Composite. Four milliliters of graphite oxide aqueous suspension (10.0 mg mL^{-1}) was diluted to 1.0 mg mL^{-1} with double distilled water and then sonicated for 20 min to achieve a brown homogeneous graphene oxide aqueous suspension. Afterward, 160 mg of silicon nanoparticles (<300 nm, Top Vendor Science & Technology Co., Ltd.) were dispersed in 20 mL of water via 40 min sonication (KQ3200DE, 40 kHz). Then, the achieved Si nanoparticles aqueous suspension was added into the above graphene oxide aqueous suspension, and the obtained mixture was sonicated for 10 min to obtain a uniform Si nanoparticles/graphene oxide aqueous suspension. The resulting homogeneous aqueous suspension was lyophilized, followed by reduction in a crucible in a tube furnace at 700 °C for 2 h under H_2 (5 vol%)/Ar (95 vol%) atmosphere with a heating rate of 2 °C min^{-1}, treatment with 20% HF water/ethanol solution, and drying under vacuum at 80 °C to finally obtain Si/G composite.

Synthesis of Carbon Nanoparticle/Graphene Composite. Two milliliters of graphite oxide aqueous suspension (10.0 mg mL^{-1}) was diluted to 1.0 mg mL^{-1} with double distilled water, then 20 mg of carbon nanoparticles (~40 nm in diameter, Super-P, Timcal) was added into the graphite oxide aqueous suspension and the obtained mixture was sonicated for 20 min to achieve a black homogeneous carbon nanoparticles/graphene oxide aqueous suspension. Afterward, the resulting homogeneous aqueous suspension was lyophilized, followed by reduction in a crucible in a tube furnace at 700 °C for 2 h under H_2 (5 vol%)/Ar (95 vol%) atmosphere with a heating rate of 2 °C min^{-1} to finally obtain C/G composite.

Structural and Electrochemical Characterizations. SEM was conducted on a JEOL 6701 scanning electron microscope operated at 10 kV. TEM and HRTEM were performed using a Tecnai G2 F20 U-TWIN transmission electron microscope operated at 200 kV. EDX analysis was carried out with an EDAX system attached to the Tecnai G2 F20 U-TWIN microscope. XRD measurements were performed on a Rigaku D/max2500 diffractometer using CuKα radiation. XPS analysis was carried out with an ESCALab220i-XL electron spectrometer from VG Scientific using 300W AlKα radiation. TG analysis was conducted on a TA-Q50 instrument. Nitrogen adsorption and desorption isotherms at 77.3 K were achieved with a Nova 2000e surface area-pore size analyzer. Electrochemical experiments were performed using Swagelok-type cells. To prepare Si−C/G, Si/G, and C/G electrodes, we mixed the active materials and poly(vinylidene fluoride) (PVDF) with a mass ratio of 90:10 into a homogeneous slurry with mortar and pestle. To prepare Si/G + C electrodes, we mixed the Si/G, carbon nanoparticles (~40 nm in diameter, Super-P, Timcal), and PVDF with mass ratio of 63.8:26.2:10 into a homogeneous slurry with mortar and pestle. Then, the obtained slurrys were pasted onto pure Cu foils (99.9%, Goodfellow). The loading mass of active materials is about 10 mg cm^{-2}. The electrolyte was 1 M $LiPF_6$ in EC/DMC (1:1 v/v) (Tianjing Jinniu Power Sources Material Co. Ltd.) plus 2 wt % vinylene carbonate (VC). Glass fibers (GF/D) from Whatman were utilized as separators and pure lithium

metal foil (Aldrich) was used as the counter electrode. The Swagelok-type cells were assembled in an argon-filled glovebox. Cyclic voltammetry was carried out on a Voltalab 80 electrochemical workstation at a scan rate of 0.1 mV s^{-1}. The discharge and charge measurements of the batteries were performed on an Arbin BT2000 system in the fixed voltage window between 0.005 and 1 V at room temperature. Electrochemical impedance spectral measurements were recorded on a PARSTAT 2273 advanced electrochemical system over the frequency range from 100 kHz to 10 mHz.

RESULTS AND DISCUSSION

As demonstrated in Figure 1, the fabrication of the Si−C/G composite involves two steps. First, graphene oxide and carbon nanoparticles are mixed in water via sonication. The graphene oxide is composed of hydrophobic polyaromatic domains to interact with carbon nanoparticles and hydrophilic hydroxyl and carboxyl acid groups for dispersion in water.[29,34] A stable structure of carbon nanoparticles/graphene oxide can form with carbon nanoparticles well dispersed and adsorbed on the graphene oxide. Second, an aqueous suspension of Si nanoparticles is introduced to the as-prepared C/G composite followed by further sonication. After a series of procedures including freeze-drying, thermal reduction, and HF treatment, the final product as Si−C/G composite can be collected. Details of the synthesis can be found in the Experimental Section.

To investigate structure built by the graphene and carbon nanoparticles, we first perform the transmission electron microscopy (TEM) analysis on the C/G composite as shown in Figure 2a. The stringlike carbon nanoparticles are well dispersed in the graphene framework and they form a perfect dispersion with no obvious aggregation. It is interesting that under the SEM images in Figure 2b, we can only observe wrinkled and rough graphene nanosheets with just a few spherical nanoparticles. It seems that the majority of these nanoparticles are under the cover of the graphene nanosheets. Similarly, a homogeneous admixture can be formed after the introduction of silicon nanoparticles. As shown in Figure 2c, the Si−C/G composite includes Si nanoparticles, string-like carbon nanoparticles and graphene sheets. The energy dispersive X-ray spectroscopy (EDX) measurement confirms the existence of Si in the Si−C/G composite (Figure 2d). The thermal gravimetric (TG) analysis reveals that the Si−C/G composite contains approximately 61.3 wt % Si and 38.7 wt % carbon including graphene and carbon nanoparticles (see Figure S1 and Table S1 in the Supporting Information). In addition, we analyze the middle and edge of a Si−C/G composite with HRTEM technique. The HRTEM image of the middle part reveals that Si nanocrystals are surrounded by onionlike carbon nanoparticles,[35] and the Si nanocrystals and carbon nanoparticles are covered by wrinkled graphene sheets (Figure 2e). The HRTEM image taken at the edge of the composite shows that the Si nanocrystals and the neighboring onion-like carbon nanoparticles are well enwrapped by 2−3 nm graphene sheets (Figure 2f).

Further evidence of the uniform mixture of Si nanoparticles and string-like carbon nanoparticles encapsulated by graphene is demonstrated by the dark-field scanning transmission electron microscopy (STEM) image and EDX mappings. Figure 3a clearly shows that the graphene sheets enwrap Si nanoparticles and carbon nanoparticles well. This is also validated by the pattern from the EDX mapping of oxygen. The brown oxygen signals are mainly from residual oxygen functional groups of graphene and they cover the entire sample area (Figure 3b). Figure 3c,d shows the EDX mappings of carbon and silicon, respectively. Figure 3e shows the overlay of Figure 3d and Figure 3e, indicating that the string-like carbon nanoparticles are well mixed with Si nanoparticles (Figure 3c−e).

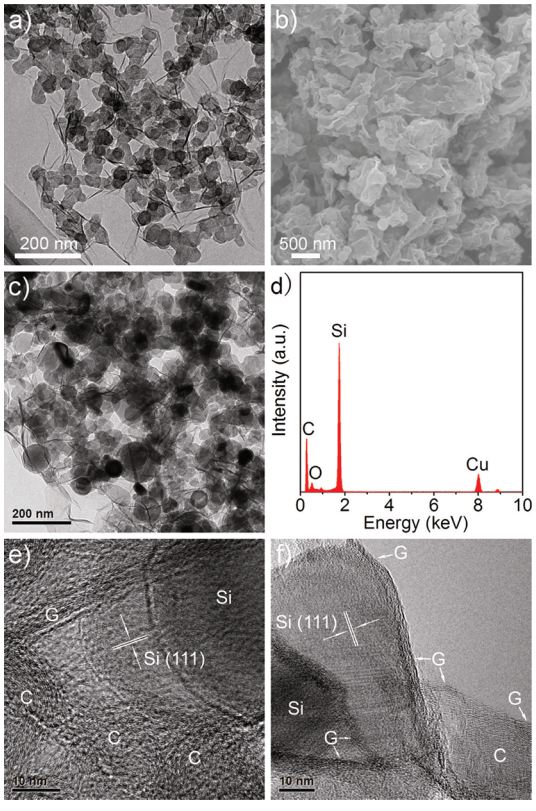

Figure 2. (a) TEM image of the C/G composite; (b, c) SEM and TEM images of the Si−C/G composite; (d) EDX spectrum of the Si−C/G composite; (e, f) HRTEM images of the Si−C/G composite.

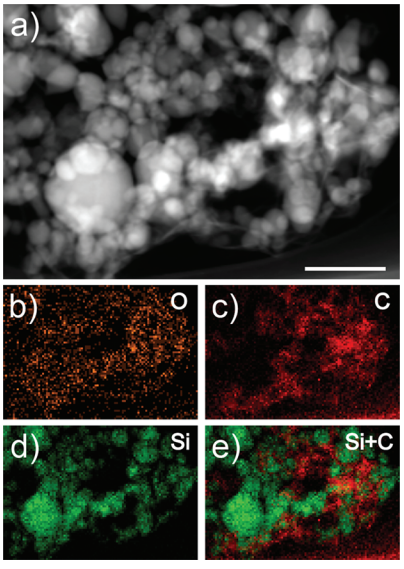

Figure 3. (a) Dark-field STEM image of the Si−C/G composite; (b−d) EDX mappings of oxygen, carbon, and silicon of the Si−C/G composite; (e) overlay of c and d; scale bar is 200 nm.

dx.doi.org/10.1021/am3005576 | ACS Appl. Mater. Interfaces 2012, 4, 2824−2828

X-ray diffraction (XRD) patterns of Si−C/G composite, carbon nanoparticles, and graphene sheets are shown in Figure S2 in the Supporting Information. Obviously, Si nanoparticles remain crystalline in the Si−C/G composite after sonication and heat treatment. The tiny peaks around 26° as enlarged for Si−C/G composite are characteristic for carbon nanoparticles and graphene sheets.[36,37] The N_2 adsorption/desorption isotherms of the Si−C/G composite exhibit a type IV pattern with an associated H3 type hysteresis loop, revealing a mesoporous structure of the composite (see Figure S3a in the Supporting Information). The Barrett−Joyner−Halenda (BJH) pore-size distribution shows that such mesopores are around 4.2 nm in diameter (see Figure S3b in the Supporting Information). X-ray photoelectron spectroscopy (XPS) survey of the Si−C/G composite confirms that the GO have been successfully reduced to graphene during the thermal reduction (see Figure S4 in the Supporting Information).

It can be concluded that the Si nanoparticles are well mixed with the stringlike carbon nanoparticles, and both of them are encapsulated by graphene sheets to form Si−C/G composite. Zero-dimensional (0D) carbon nanoparticles and two-dimensional (2D) graphene sheets construct efficient 3D conducting networks for Si nanoparticles. The rational design is much desirable for Si anode because it not only effectively enhances the conduction of electron but also accommodates the large volume changes of Si nanoparticles during Li insertion and extraction processes.

A typical cyclic voltammetry (CV) characterization of the Si−C/G composite is shown in Figure S5. A broad cathodic peak in the first cycle appeared at 0.77 V, indicating the formation of solid electrolyte interphase (SEI). The cathodic part of the second cycle exhibits two peaks at 0.022 and 0.20 V, corresponding to the generation of Li−Si alloy phases. The anodic part shows two peaks at 0.32 and 0.50 V, which could be assigned to the dealloying of Li−Si alloys. The results are in good agreement with the data reported before.[20]

Figure 4a shows the discharge−charge profiles of the first three cycles of the Si−C/G composite at 0.2 C (1C = 4.2 A g^{-1}) between the voltage limits of 0.005−1 V vs Li^+/Li. The initial discharge and charge capacities are 2959 and 4572 mA h g^{-1} based on the mass of Si, respectively, leading to a Coulombic efficiency of 64.7%. The irreversible capacity loss of the Si−C/G composite can be ascribed to the formation of the SEI and the existence of carbon nanoparticles and graphene, whose initial discharge capacity and Coulombic efficiency are 1005 mA h g^{-1} and 20.5%, respectively (see Figure S6 in the Supporting Information). The Coulombic efficiency becomes stable in the range of 96−100% after the second cycle. As shown in Figure 4b, the Si−C/G composite exhibits excellent cycle performance. The reversible capacity of Si−C/G composite is still as high as 1521 mA h g^{-1} even after 200 cycles.

To show the advantage of the 3D conducting networks, we compared the cycling performance of Si/G electrodes and Si/G + C electrodes (see preparation details in the Experimental Section) under the same conditions. The Si/G composite was synthesized by a similar method combining freeze-drying and thermal reduction as previously reported.[24] It is found that severe aggregation of Si nanoparticles becomes inevitable in the as-obtained Si/G composite (Figure S7, see the Supporting Information) when using a high concentration solution of Si nanoparticles in the preparation process. The content of Si in the as-obtained Si/G composite is about 84.7 wt % (Table S2,

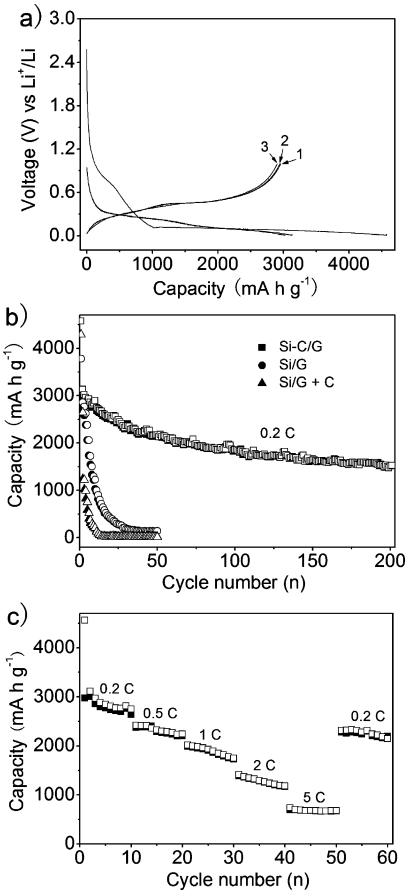

Figure 4. (a) Galvanostatic discharge−charge profiles of the first three cycles, (b) cycling performance of the Si−C/G composite, and (c) rate capability of the Si−C/G composite.

see the Supporting Information). Electrochemical test results indicate that both the Si/G electrodes and the Si/G + C electrodes exhibit a rapid capacity fading (Figure 4b), which could be attributed to the large volume changes of these aggregated and irregular Si nanoparticles during Li insertion and extraction, leading to an electrical disconnection among nanoparticles. In the contrast, in the case of the Si−C/G composite, the additional of carbon nanoparticles can effectively alleviate the aggregation of Si nanoparticles by separating them from each other (see Figure 3), helps to form an efficient 3D conducting networks together with graphene sheets, leading to the much improved cycling performance compared with the Si/G and the Si/G+C electrodes. Note that Si nanoparticles (<300 nm) used here are mechanically produced from bulk polycrystalline Si. They are low cost, commercially available, but in different sizes.

The rate capability of the Si−C/G composite was also evaluated from 0.2 to 5 C. As shown in Figure 4c, the Si−C/G composite can deliver reversible capacities of about 1747, 1178, and 677 mA h g^{-1} at a discharge rate of 1C, 2C, and 5C, respectively. The improved electrochemical performance of Si−C/G composite could be ascribed to the following reasons. First, the string-like carbon nanoparticles are well mixed with Si nanoparticles and it could offer sufficient electrons to the Si nanoparticles within graphene. Second, the graphene frameworks could buffer large volume changes from Li−Si alloying and dealloying reactions and maintain the integrity of Si−C/G electrode.

The electrochemical impedance spectra (EIS) of Si−C/G electrodes were investigated to obtain further insights of the improved cycling performance. The Nyquist plots show a depressed semicircle at high frequency and a straight line at low frequency.The charge-transfer resistances of the electrode can be determined by the diameters of these semicircleas. It is 13.1Ω for the freshly assembled cell and then it increases to 44.5 Ω and 48.7 Ω after three cycles and 100 cycles, respectively. It is obvious that extended cycles up to 100 does not increase the charge-transfer resistance much, indicating that the 3D conducting networks of Si−C/G composite is pretty robust (see Figure S8 in the Supporting Information).

CONCLUSIONS

In summary, we have realized improved electrode performance of Si nanoparticles by introducing 3D conducting networks built by carbon nanoparticles and graphene sheets. The string-like carbon nanoparticles alleviate the aggregation of Si nanoparticles, and enhance the electrical connection between Si nanoparticles and graphene sheets, while the graphene frameworks accommodate large volume changes of Si nanoparticles. The as-obtained Si−C/G composite shows a much improved cycling performance (ca. 1521 mA h g^{-1} after 200 cycles) and a good high-rate capability. The whole approach is simple, yet very effective for extensive use of Si nanoparticles as anode materials, and owing to its versatility, could also be extended to other anode and cathode materials with large volume changes used in lithium-ion batteries.

ASSOCIATED CONTENT

Supporting Information

TG analysis, XRD patterns, nitrogen adsorption/desorption isotherms, pore-size distribution, XPS spectra, CV curves, cycling performance, TEM image, and Nyquist plots of the samples. This material is available free of charge via the Internet at http://pubs.acs.org.

AUTHOR INFORMATION

Corresponding Author

*E-mail: ygguo@iccas.ac.cn.

Notes

The authors declare no competing financial interest.

ACKNOWLEDGMENTS

This work was supported by the National Basic Research Program of China (Grant Nos. 2011CB935700, 2009CB930400, and 2012CB932900), the National Natural Science Foundation of China (Grants 91127044 and 21121063), and the Chinese Academy of Sciences.

REFERENCES

(1) Armand, M.; Tarascon, J.-M. *Nature* **2008**, *451*, 652−657.
(2) Maier, J. *Nat. Mater.* **2005**, *4*, 805−815.
(3) Kang, B.; Ceder, G. *Nature* **2009**, *458*, 190−193.
(4) Ke, F. S.; Huang, L.; Wei, H.-B.; Cai, J.-S.; Fan, X.-Y.; Yang, F.-Z.; Sun, S.-G. *J. Power Sources* **2007**, *170*, 450−455.
(5) Cao., F.-F.; Guo, Y.-G.; Zheng., S.-F.; Wu., X.-L.; Jiang., L.-Y.; Bi., R.-R.; Wan., L.-J.; Maier., J. *Chem. Mater.* **2010**, *22*, 1908−1914.
(6) Liang, C.; Dudney, N. J.; Howe, J. Y. *Chem. Mater.* **2009**, *21*, 4724−4730.
(7) Guo, Y.-G.; Hu, J.-S.; Wan, L.-J. *Adv. Mater.* **2008**, *20*, 2878−2887.
(8) Lou, X. W.; Wang, Y.; Yuan, C.; Lee, J. Y.; Archer, L. A. *Adv. Mater.* **2006**, *18*, 2325−2329.
(9) Dong, S.; Chen, X.; Gu, L.; Zhou, X.; Xu, H.; Wang, H.; Liu, Z.; Han, P.; Yao, J.; Wang, L.; Cui, G.; Chen, L. *ACS Appl. Mater. Interfaces* **2011**, *3*, 93−98.
(10) Hu, Y.-S.; Demir-Cakan, R.; Titirici, M.-M.; Müller, J.-O.; Schlögl, R.; Antonietti, M.; Maier, J. *Angew. Chem., Int. Ed.* **2008**, *47*, 1645−1649.
(11) Shu, J.; Li, H.; Yang, R.; Shi, Y.; Huang, X. *Electrochem. Commun.* **2006**, *8*, 51−54.
(12) Ma, H.; Cheng, F.; Chen, J.; Zhao, J.; Li, C.; Tao, Z.; Liang, J. *Adv. Mater.* **2007**, *19*, 4067−4070.
(13) Jia., H.; Gao, P.; Yang, J.; Wang, J.; Nuli, Y.; Yang, Z. *Adv. Energy Mater.* **2011**, *1*, 1036−1039.
(14) Bates, J. B.; Dudney, N. J.; Neudecker, B.; Ueda, A.; Evans, C. D. *Solid State Ionics* **2000**, *135*, 33−45.
(15) Kim, H.; Han, B.; Choo, J.; Cho, J. *Angew. Chem., Int. Ed.* **2008**, *47*, 10151−10154.
(16) Yu, Y.; Gu, L.; Zhu, C.; Tsukimoto, S.; van Aken, P. A.; Maier, J. *Adv. Mater.* **2010**, *22*, 2247−2250.
(17) Chan, C. K.; Peng, H.; Liu, G.; Mcllwrath, K.; Zhang, X. F.; Huggins, R. A.; Cui, Y. *Nat. Nanotechnol.* **2008**, *3*, 31−35.
(18) Hertzberg, B.; Alexeev, A.; Yushin, G. *J. Am. Chem. Soc.* **2010**, *132*, 8548−8549.
(19) Cao, F.-F.; Deng, J.-W.; Xin, S.; Ji, H.-X.; Schmidt, O. G.; Wan, L.-J.; Guo, Y.-G. *Adv. Mater.* **2011**, *23*, 4415−4420.
(20) Yao, Y.; McDowell, M. T.; Ryu, I.; Wu, H.; Liu, N.; Hu, L.; Nix, W. D.; Cui, Y. *Nano Lett.* **2011**, *11*, 2949−2954.
(21) Ng, S.-H.; Wang, J.; Wexler, D.; Konstantinov, K.; Guo, Z.-P.; Liu, H.-K. *Angew. Chem., Int. Ed.* **2006**, *45*, 6896−6899.
(22) Dimov, N.; Kugino, S.; Yoshio, M. *Electrochim. Acta* **2003**, *48*, 1579−1587.
(23) Lee, J. K.; Smith, K. B.; Hayner, C. M.; Kung, H. H. *Chem. Commun.* **2010**, *46*, 2025−2027.
(24) Zhou, X.; Yin, Y.-X.; Wan, L.-J.; Guo, Y.-G. *Chem. Commun.* **2012**, *48*, 2198−2200.
(25) Xiang, H.; Zhang, K.; Ji, G.; Lee, J. Y.; Zou, C.; Chen, X.; Wu, J. *Carbon* **2011**, *49*, 1787−1796.
(26) Liu, Y.; Matsumura, T.; Imanishi, N.; Hirano, A.; Ichikawa, T.; Takeda, Y. *Electrochem. Solid-State Lett.* **2005**, *8*, A599−A602.
(27) Wang, Y.; Li, Y.; Tang, L.; Lu, J.; Li, J. *Electrochem. Commun.* **2009**, *11*, 889−892.
(28) Zhou, X.; Wu, T.; Hu, B.; Yang, G.; Han, B. *Chem. Commun.* **2010**, *46*, 3663−3665.
(29) Wang, H.; Yang, Y.; Liang, Y.; Robinson, J. T.; Li, Y.; Jackson, A.; Cui, Y.; Dai, H. *Nano Lett.* **2011**, *11*, 2644−2647.
(30) Zhu, Y.; Murali, S.; Cai, W.; Li, X.; Suk, J. W.; Potts, J. R.; Ruoff, R. S. *Adv. Mater.* **2010**, *22*, 3906−3924.
(31) Yang, S.; Feng, X.; Ivanovici, S.; Müllen, K. *Angew. Chem., Int. Ed.* **2010**, *49*, 8408−8411.
(32) Myung, S.; Solanki, A.; Kim, C.; Park, J.; Kim, K. S.; Lee, K.-B. *Adv. Mater.* **2011**, *23*, 2221−2225.
(33) Hummers, W. S.; Offeman, R. E. *J. Am. Chem. Soc.* **1958**, *80*, 1339−1339.
(34) Cote, L. J.; Kim, J.; Zhang, Z.; Sun, C.; Huang, J. *Soft Matter* **2010**, *6*, 6096−6101.
(35) Pech, D.; Brunet, M.; Durou, H.; Huang, P.; Mochalin, V.; Gogotsi, Y.; Taberna, P.-L.; Simon, P. *Nat. Nanotechnol.* **2010**, *5*, 651−654.
(36) Chen, X.-H.; Wu, G.-T.; Deng, F.-M.; Wang, J.-X.; Yang, H.-S.; Wang, M.; Lu, X.-N.; Peng, J.-C.; Li, W.-Z. *Acta Phys. Sin.* **2001**, *50*, 1264−1267.
(37) Xu, Y.; Bai, H.; Lu, G.; Li, C.; Shi, G. *J. Am. Chem. Soc.* **2008**, *130*, 5856−5857.